Naval Research Laboratory

Washington, DC 20375-5320

NRL/MR/6790--93-7384

A Tunable Compact High Power Far-Infrared Grating Free-Electron Laser

B. HAFIZI

Icarus Research
7113 Exfair Road
Bethesda, MD 20814

P. SPRANGLE
A. FISHER

Beam Physics Branch
Plasma Physics Division

September 13, 1993

REPORT DOCUMENTATION PAGE

Form Approved
OMB No. 0704-0188

1. AGENCY USE ONLY *(Leave Blank)*	2. REPORT DATE	3. REPORT TYPE AND DATES COVERED
	September 13, 1993	Interim

4. TITLE AND SUBTITLE

A Tunable Compact High Power Far-Infrared Grating Free-Electron Laser

5. FUNDING NUMBERS

6. AUTHOR(S)

B. Hafizi,* P. Sprangle and A. Fisher

7. PERFORMING ORGANIZATION NAME(S) AND ADDRESS(ES)

Naval Research Laboratory
Washington, DC 20375-5320

8. PERFORMING ORGANIZATION REPORT NUMBER

NRL/MR/6790--93-7384

9. SPONSORING/MONITORING AGENCY NAME(S) AND ADDRESS(ES)

Office of Naval Research
800 North Quincy Street
Arlington, VA 22217-5660

10. SPONSORING/MONITORING AGENCY REPORT NUMBER

11. SUPPLEMENTARY NOTES

*Icarus Research, 7113 Exfair Road, Bethesda, MD 20814

12a. DISTRIBUTION/AVAILABILITY STATEMENT

Approved for public release; distribution unlimited.

12b. DISTRIBUTION CODE

13. ABSTRACT *(Maximum 200 words)*

The linear and nonlinear operation of a multiwave grating free-electron laser is described. The radiation is generated by the passage of an annular electron beam through a coaxial waveguide, the central conductor being in the form of a corrugated cylinder. The model includes the effects of self-field forces, beam emittance and gyromotion of electrons in a guide magnetic field. The efficiency is determined by numerical simulation and compared with analytical estimates. A compact source that is tunable in the wavelength band 35-55 μm with output in the kilowatt range is shown to be feasible.

14. SUBJECT TERMS

Free-electron laser
Tunable
Grating
Compact
Coaxial waveguide structure
Hollow beam

15. NUMBER OF PAGES

34

16. PRICE CODE

17. SECURITY CLASSIFICATION OF REPORT	18. SECURITY CLASSIFICATION OF THIS PAGE	19. SECURITY CLASSIFICATION OF ABSTRACT	20. LIMITATION OF ABSTRACT
UNCLASSIFIED	UNCLASSIFIED	UNCLASSIFIED	SAR

NSN 7540-01-280-5500

Standard Form 298 (Rev. 2-89)
Prescribed by ANSI Std 239-18
298-102

CONTENTS

A TUNABLE COMPACT HIGH POWER FAR-INFRARED GRATING FREE-ELECTRON LASER

I. Introduction

High-power generators of coherent radiation in the infrared (IR) are under consideration in a number of laboratories. An example of this is a free-electron source of radiation based on the Smith-Purcell mechanism.[1] In a free-electron laser (FEL) based on the Smith-Purcell mechanism an electron beam interacts with the slow-wave structure of a metallic grating. The interaction leads to bunching of the beam and amplification of radiation.[2-15] Since only moderate energy ($<$ few MeV) electron beams are required, the grating FEL has the potential of developing into a truly compact, benchtop source of IR radiation.

In Ref. 15 an analysis of a grating FEL in planar geometry, employing a sheet electron beam of finite thickness, has been presented. Experiments at the Naval Research Laboratory with sheet beam configurations have been hampered by deformation and warping at the beam edges. New experiments, using annular electron beams to avoid edge problems, are presently underway, aimed at the generation of far-IR radiation. To increase the power handling capability, large, overmoded structures (i.e., with waveguide radius $\gg$ free-space wavelength) are adopted. This is referred to as multiwave operation.

A schematic of the experimental set-up is shown in Fig. 1. A hollow, cylindrical electron beam from a cold, field-emission gun is made to pass through a coaxial waveguide, the central conductor being in the form of a grating. The entire system, including the electron gun, is immersed in a uniform axial magnetic field in order to achieve confined flow of the beam. The discussion here is limited to the case

Manuscript approved August 13, 1993.

in which the electrons interact with a spatial harmonic whose group velocity is nearly zero and consequently the energy drained from the radiation field is reduced. This is illustrated in Fig. 2 which indicates one branch of the Brillouin diagram for the three lowest spatial harmonics of a coaxial resonator with a smooth outer conductor and a corrugated central conductor. Outcoupling may be accomplished by diffraction (quasioptical).

A linear and a fully nonlinear analysis of an annular electron beam grating FEL with allowance for electron beam emittance and gyromotion in a guide magnetic field is presented here. The model is used to obtain design parameters for experiments aimed at the generation of 45 μm radiation using a 105 kV beam. The efficiency is determined by means of numerical simulation and compared with analytical estimates. Tuning characteristics of this source over the wavelength band 35-55 μm are presented.

II. Electronic and Circuit Equations

The purpose of this section is to derive the equations that describe the motion of electrons in the electromagnetic field inside an open resonator formed by a coaxial waveguide with a corrugated center conductor, the entire system, including the electron gun, being immersed in an axial magnetic guide field. Cylindrical coordinates are denoted by (r, φ, z) with the z axis lying along the axis of the waveguide. (Fig. 1.) The discussion is limited to TM modes since the electrons streaming through the resonator are expected to interact strongly with axial electric fields. For simplicity, only azimuthally symmetric TM_{0nn} modes are considered.

A. Circuit Dispersion Relation

The z component of the resonator electric field can be written as

$$\mathcal{E}_z(r,z,t) = E_z(r,z)\exp(-i\omega t) + \text{c.c.}, \tag{1}$$

where $\omega = 2\pi c/\lambda$ is the frequency, λ is the free-space wavelength and $E_z(r,z)$ represents the spatial variation of the field. In the region above the grating surface and bounded by the outer conductor, $r_g \leq r \leq R$, E_z is expressed as a sum of all the even spatial harmonics:

$$E_z(r,z) = A_0 J_0(k_0 r) + B_0 Y_0(k_0 r) + \sum_{n=1}^{\infty} \cos(2\pi\, n\, z/d)\,[A_n I_0(\kappa_n r) + B_n K_0(\kappa_n r)], \tag{2}$$

where d is the grating pitch, J_0 and Y_0 are the ordinary Bessel functions of first and second kind, respectively, of order 0 and I_0 and K_0 are the modified Bessel

functions of first and second kind, respectively, of order 0. In Eq. (2) A_0 and B_0 are the amplitudes of the $n = 0$ (i.e., fundamental) spatial harmonic, with wavenumber k_0 and A_n and B_n are the amplitudes of the nth spatial harmonic, with wavenumber κ_n. The wavenumbers k_0 and κ_n will be identified presently.

The simplest solution in the region $r_g - b \leq r \leq r_g$, where b is the corrugation depth, is a TEM standing wave in each slot:[16]

$$E_z(r) = C_0 J_0(k_0 r) + D_0 Y_0(k_0 r). \tag{3}$$

The assumption of a TEM mode in the slots is strictly valid for $s \ll \lambda$, where s is the groove width.

The other relevant components of the electromagnetic field (i.e., B_φ and E_r) may be obtained from Maxwell's equations. It follows from the wave equation that $k_0 = \omega/c$ and

$$\kappa_n = \left[(2\pi n/d)^2 - (\omega/c)^2\right]^{1/2}, \quad (n = 1, 2, 3, \ldots).$$

From the boundary condition on E_z one can express all the amplitudes in terms of A_0; in particular,

$$A_n = 2A_0 \frac{\sin(\pi n s/d)}{\pi n s/d} \frac{J_0(k_0 r_g) - \frac{J_0(k_0 R)}{Y_0(k_0 R)} Y_0(k_0 r_g)}{I_0(\kappa_n r_g) - \frac{I_0(\kappa_n R)}{K_0(\kappa_n R)} K_0(\kappa_n r_g)}, \tag{4}$$

$$B_n = -A_n \frac{I_0(\kappa_n R)}{K_0(\kappa_n R)}, \tag{5}$$

$$B_0 = -A_0 \frac{J_0(k_0 R)}{Y_0(k_0 R)}. \tag{6}$$

Finally, from the continuity condition on B_φ one obtains the dispersion relation for the circuit:

$$\frac{J_1(k_0 r_g) - \frac{J_0(k_0 R)}{Y_0(k_0 R)} Y_1(k_0 r_g)}{J_0(k_0 r_g) - \frac{J_0(k_0 R)}{Y_0(k_0 R)} Y_0(k_0 r_g)} = \frac{d}{s} \frac{J_1(k_0 r_g) - \frac{J_0[k_0(r_g - b)]}{Y_0[k_0(r_g - b)]} Y_1(k_0 r_g)}{J_0(k_0 r_g) - \frac{J_0[k_0(r_g - b)]}{Y_0[k_0(r_g - b)]} Y_0(k_0 r_g)}$$

$$-2 \sum_{n=1}^{\infty} \frac{k_0}{\kappa_n} \frac{I_1(\kappa_n r_g) + \frac{I_0(\kappa_n R)}{K_0(\kappa_n R)} K_1(\kappa_n r_g)}{I_0(\kappa_n r_g) - \frac{I_0(\kappa_n R)}{K_0(\kappa_n R)} K_0(\kappa_n r_g)} \left[\frac{\sin(\pi n s/d)}{\pi n s/d} \right]^2 . \tag{7}$$

All the waveguide dimensions is this expression may be scaled to the grating pitch, d, and the transcendental equation solved for $k_0 d$.

In the following it will be assumed that only the $n = 1$ spatial harmonic is resonant with the electrons and therefore the only relevant component of the slow-wave structure. That is, $\lambda/d \approx 1/\beta_z$, where $\beta_z = v_z/c$ is the ratio of the axial electron velocity to the speed of light. This permits us to disregard the interaction of all but the $n = 1$ spatial harmonic with the electrons.

B. Synchrotron and Betatron Equations of Motion

In the synchrotron phase space, the equations of motion of the jth electron, of charge $-|e|$ and rest mass m, interacting with the $n = 1$ spatial harmonic are given by

$$\frac{d\psi_j}{dt} = 2\pi c \beta_{zj}/d - \omega, \tag{8}$$

$$\frac{d\gamma_j}{dt} = -\frac{|e|\beta_{zj}}{2mc} [A_1 I_0(\kappa_1 r_j) + B_1 K_0(\kappa_1 r_j)] \exp(i\psi_j) + \mathcal{O}\left(\frac{v_\perp}{v_z}\right) + \text{c.c.}, \tag{9}$$

where $\psi_j = 2\pi z_j/d - \omega t$ and $v_\perp$ is the electron velocity in the (r, φ) plane.

In the betatron phase space, it is assumed that the motion of the electrons is not directly affected by the radiation field. The forces in the betatron phase space arise from the self-electric and -magnetic fields plus that due to the axial guide magnetic field, B_0. Since the radius of the electron beam, r_b, is much greater than the width of the electron beam, Δr_b, or the electron gyroradius, it is permissible to consider the hollow cylindrical beam to constitute an infinite strip beam. For a strip beam the equations of motion of an electron are

$$\frac{d^2x}{dt^2} - \Omega_b^2 x = -\Omega_0 \frac{dy}{dt}, \tag{10}$$

$$\frac{d^2y}{dt^2} = \Omega_0 \frac{dx}{dt}, \tag{11}$$

where $x \approx r - r_b$, $y \approx r_b\varphi$, $\Omega_0 = |e|B_0/\gamma mc$ is the relativistic gyrofrequency in the guide field, $\gamma = (1 - v^2/c^2)^{-1/2}$, $\Omega_b = (4\pi n_b|e|^2/\gamma\gamma_z^2 m)^{1/2}$ is the relativistic plasma frequency and n_b is the beam density. The electrons are emitted from the surface of an immersed cathode with finite emittance. Denoting the conserved canonical momentum by $P_y = \gamma m(dy/dt - \Omega_0 x)$, Eq. (10) simplifies to

$$\frac{d^2x}{dt^2} + \Omega^2 x = -\frac{\Omega_0 P_y}{\gamma m}, \tag{12}$$

where $\Omega^2 = \Omega_0^2 - \Omega_b^2$. To solve Eq. (12) we put[17]

$$x(t) = \xi X(t)\exp[i\phi(t) + \theta] - \frac{\Omega_0 P_y}{\gamma m \Omega^2}, \tag{13}$$

and substitute in to obtain equations for $X(t)$ and $\phi(t)$. In Eq. (13) X and ϕ are the same for all electrons whereas $0 \leq \xi \leq 1$ and $0 \leq \theta \leq 2\pi$ are parameters that

may be chosen to represent any desired distribution of electrons. The equations for X and ϕ are

$$\frac{d^2X}{dt^2} - X\left(\frac{d\phi}{dt}\right)^2 + \Omega^2 X = 0, \tag{14}$$

$$X^2\frac{d\phi}{dt} = \epsilon v_z, \tag{15}$$

where ϵ is the (unnormalized) emittance of the electron beam. Substituting Eq. (15) into Eq. (14), one obtains an equation for the beam envelope:

$$\frac{d^2X}{dt^2} + \Omega^2 X - \frac{\epsilon^2 v_z^2}{X^3} = 0. \tag{16}$$

For a matched electron beam $X(t) = X_b =$ constant and Eq. (16) may be solved to obtain $X_b = (\epsilon v_z/\Omega)^{1/2}$. Making use of this, the betatron motion is given by

$$x = \xi\left(\frac{\epsilon v_z}{\Omega}\right)^{1/2}\cos(\Omega t + \theta) - \frac{\Omega_0 P_y}{\gamma m \Omega^2}, \tag{17}$$

$$y = \xi\frac{\Omega_0}{\Omega}\left(\frac{\epsilon v_z}{\Omega}\right)^{1/2}\sin(\Omega t + \theta) - \frac{\Omega_b^2}{\Omega^2}\frac{P_y}{\gamma m}t, \tag{18}$$

where the last term in Eq. (18) represents the $E \times B$ precession in the azimuthal direction. If t_0 is the time at which the electron is born on the cathode, Eq. (17) may be rewritten as

$$x = x_0 + \xi\left(\frac{\epsilon v_z}{\Omega}\right)^{1/2}[\cos(\Omega t + \theta) - \cos(\Omega t_0 + \theta)],$$

where x_0 is the x-coordinate of the electron on the cathode at the instant of emission. It follows that the full width of the electron beam, Δr_b, is determined by i) The spread in x_0, i.e., the region of beam formation on the cathode and ii) By the

emittance, through $(\epsilon v_z/\Omega)^{1/2}$. Note that in the limit $\Omega_0 \gg \Omega_b$ the width X_b is determined by the normalized emittance, $\gamma\beta_z\epsilon$.

Finite emittance causes inhomogeneous broadening of the emitted radiation which, upon using Eq. (8), is expressible as

$$(\delta\lambda/\lambda)_{inhom} \approx |\delta\beta_z/\beta_z|,$$

where $\delta\beta_z$ is the spread in β_z. Noting that $v_z^2 = v^2 - v_\perp^2$, where v is the electron speed and $v_\perp^2 = [(dx/dt)^2 + (dy/dt)^2]$, it follows that $| < \delta v_z > | \approx < v_\perp^2 > /2v$, where $<>$ indicates an average over the electron distribution. Next, evaluating $v_\perp$ with the aid of Eqs. (17) and (18) one obtains

$$\left(\frac{\delta\lambda}{\lambda}\right)_{inhom} = \frac{1}{3\beta_z^2}\left(\frac{\Omega X_b}{2c}\right)^2\left[1 + \left(\frac{\Omega_0}{\Omega}\right)^2\right] + \mathcal{O}\left(\frac{\Omega_b^4}{\Omega_0^4}\right), \tag{19}$$

where it has been assumed that ξ is uniformly distributed in the interval [0,1]. Note that the spread in the axial energy, $< \delta\gamma_z > mc^2$, is obtained from the relation $\delta\gamma_z = \beta_z\gamma_z^3\delta\beta_z$.

Equations (8), (9), (17) and (18) form a closed system of equations for the analysis of the electron dynamics. They form the basis for the numerical results presented in **Sec. III**. It is useful at this point to derive the 'pendulum' equation[18] for the phase by neglecting the betatron motion. Setting $v_\perp = 0$ and $\gamma = \gamma_z$, Eqs. (8) and (9) can be combined into a single equation for ψ_j:

$$\frac{d^2\psi_j}{dt^2} = -\frac{\pi|e|}{\gamma_{zj}^3 md}[A_1 I_0(\kappa_1 r_j) + B_1 K_0(\kappa_1 r_j)]\exp(i\psi_j) + c.c. \tag{20}$$

Equation (20) shows that the motion of an electron consists of synchrotron oscillations which take place in the potential well formed by the electric field of the spatial harmonic.

C. Power

The small-signal analysis of Eq. (20) proceeds by taking A_1, B_1 and γ_z as constants and solving the equation iteratively, assuming that the right-hand side is a small term. From the small-signal analysis, the power radiated by an electron beam of thickness Δr_b is given by[5,12]

$$\frac{d\mathcal{E}_{rad}}{dt} = \frac{\omega}{8}\frac{I_b[A]}{I_0}\left(\frac{L_z}{\beta_z\gamma_z}\right)^3 g(\Theta)\int_{r_g}^{r_g+\Delta r_b}\frac{dr}{\Delta r_b}|E_{z1}|^2, \tag{21}$$

where $I_0 = 1.7\times10^4$, $I_b[A]$ is the beam current in Ampères, $g(\Theta) \equiv d(\sin\Theta/\Theta)^2/d\Theta$,

$$\Theta \equiv \left(\frac{\omega}{v_z} - \frac{2\pi}{d}\right)\frac{L_z}{2}, \tag{22}$$

L_z is the interaction length along the z axis and E_{z1} is the term corresponding to $n = 1$ in the summation in Eq. (2).

D. Start-Oscillation Condition and Gain

In the configuration indicated in Fig. 1 the coaxial waveguide forms an open resonator oscillator. If Q_L denotes the loaded quality factor of the resonator, the start-oscillation condition is expressed by

$$\frac{d\mathcal{E}_{rad}}{dt} = \frac{\omega}{Q_L}\mathcal{E}_{rad}, \tag{23}$$

where $\mathcal{E}_{rad}$, the total radiation energy stored in the optical cavity, is given by

$$\mathcal{E}_{rad} \approx \frac{L_z(R-r_g)}{\pi k_0}\left\{\frac{A_0^2}{\sin^2(k_0R-\frac{\pi}{4})}+\sum_{n=1}^{\infty}\frac{k_0A_n^2}{2\kappa_n}\left[\left(\frac{2n\pi}{\kappa_n d}\right)^2\frac{\sinh[2\kappa_n(R-r_g)]}{2\kappa_n(R-r_g)}+\left(\frac{k_0}{\kappa_n}\right)^2\right]\right\}. \tag{24}$$

In writing Eq. (24) the contribution of the field energy in the grating slots has been omitted. The loaded Q is supposed to include Ohmic losses, diffraction losses, scattering losses due to imperfections and outcoupling. According to an earlier assumption only the $n = 1$ spatial harmonic is strongly driven by the electron beam. Noting that $\kappa_1(R-r_g) \gg 1$, with the aid of Eq. (4) we identify the first term in Eq. (24) as the predominant contribution in the expression for $\mathcal{E}_{rad}$. Making use of Eqs. (4), (21), (23) and (24) one obtains an estimate for the start-oscillation current which, for $k_0(r_g-b) \gg 1$, is expressible in the form

$$I_b[A] \approx 200(-\ln R_{eff})\frac{2\pi\Delta r_b\lambda}{L_z^2}\frac{(\beta_z\gamma_z)^3}{\sin^2[k_0(R-r_g)]}\left[\frac{\pi s/d}{\sin(\pi s/d)}\right]^2\frac{\exp[2\kappa_1(R-r_g)]}{\int_{r_g}^{r_g+\Delta r_b}\frac{dr}{r}\sinh^2[\kappa_1(R-r)]}. \tag{25}$$

The integral in Eq. (25) is expressible in terms of the exponential integral and readily evaluated. In writing Eq. (25) the maximum value of $g(\Theta)$, defined prior to Eq. (22), is taken to be equal to 0.54. Additionally, the effective reflectivity R_{eff} of the optical cavity has been introduced by making use of the formula relating the reflectivity to the resonator Q, i.e., $Q_L = \omega(R-r_g)/c(-\ln R_{eff})$ (Ref. 19).

A complete set of parameters for a coaxial waveguide grating FEL using a hollow cylindrical 105 kV electron beam to generate radiation at $\lambda = 45\,\mu m$ is given in Table 1. The start-oscillation current is determined from Eq. (25) by inserting the

value of κ_1 obtained from a solution of the dispersion relation in Eq. (7). The output power is given by $\eta I_b V$, where V is the beam voltage and η, the finite-emittance efficiency, is obtained numerically in Sec. III. By definition, the gain per pass is given by $G = (L_z/v_z)\, d\ln(\mathcal{E}_{rad})/dt$ which, upon using Eq. (23), takes the form, $G = \omega L_z/Q_L v_z$. Homogeneous broadening of the radiation due to the finite interaction length is obtained by evaluating $\partial\Theta/\partial\lambda$ at constant v_z with the aid of Eq. (22):

$$\begin{aligned}(\delta\lambda/\lambda)_{hom} &= \beta_z(\lambda/L_z) \\ &\approx d/L_z,\end{aligned}$$

for a resonant interaction.

To evaluate the tunability of this source one may consider the case where the beam voltage and current are varied while the magnetic field, beam width and cavity dimensions are held fixed. Figures 3 (a)-(c) show the variation of wavelength, start-oscillation current and beam emittance with beam voltage. Shorter wavelength operation necessitates higher beam voltage as indicated in Fig. 3 (a). The higher voltage, however, leads to a larger start-oscillation current as shown in Fig. 3 (b). The slight rise in the current towards the low energy end of Fig. 3 (b) is caused by a reduction in the bunching force of the $n = 1$ spatial harmonic when the waveguide gap, $R - r_g$, approaches an integral multiple of the wavelength. Maintaining the width of the electron beam, $\Delta r_b = 2X_b = 2(\epsilon v_z/\Omega)^{1/2}$, constant–as is done here–implies a constant normalized emittance, $\gamma\beta_z\epsilon$, and hence the emittance, ϵ, varies inversely with voltage, following the curve in Fig. 3 (c).

Figure 4 (a) shows the relative axial energy spread, $\delta\gamma_z/(\gamma-1)$, on the beam. When $\delta\gamma_z/(\gamma-1)$ is sufficiently large–as it is towards the low-voltage end of Fig. 4 (a)–excitation of the oscillator from noise becomes impossible; this is discussed in Sec. III. The homogeneous broadening of the radiation is equal to 0.25% over the entire voltage range, as shown by the dashed line in Fig. 4 (b). While the inhomogeneous broadening is comparable to the homogeneous broadening at the low voltage end, the former drops off significantly with voltage, as shown by the solid line in Fig. 4 (b).

III. Design of Tunable Oscillator in the Far-Infrared

The efficiency, η, is defined as the fraction of the electron beam kinetic energy that is converted into electromagnetic radiation energy. The bandwidth of the gain function, $g(\Theta)$, sets a limit on the tolerable energy spread on the beam and hence provides an *upper* bound for the efficiency, which is given by

$$\eta = \frac{\lambda}{L_z}\frac{(\gamma_z^2 - 1)^{3/2}}{\gamma_z - 1}. \tag{26}$$

This section presents the results for the efficiency obtained from a numerical solution of Eqs. (8), (9) and (17) for the electrons comprising the beam. Subsection A discusses the example of 45 μm radiation and the 68 μm example is examined in subsection B. Subsection C examines the tuning characteristics of this source in the wavelength band 35-55 μm. In the numerical results presented here it is assumed that emittance is the predominant contribution to the width of the electron beam [cf. the discussion following Eqs. (17) and (18)].

A. 45 μm Radiation

Figure 5 (a) shows the efficiency of generation of 45 μm radiation as a function of the electric field amplitude of the fundamental spatial harmonic for a cold, infinitely thin electron beam. The efficiency in this case has been optimized with respect to the detuning Θ defined in Eq. (22) to obtain the maximum value. For the idealized case of a zero emittance, infinitely-thin beam, space-charge effects are eliminated by using a very small beam current. Inserting the corresponding numerical values,

the efficiency according to Eq. (26) is 0.66%, which is to be compared with the code result of 0.59% indicated in Fig. 5 (a).

The abscissa in Fig. 5 indicates the magnitude of the axial electric field of the fundamental spatial harmonic, A_0. The actual electric field on the conducting walls of the waveguide at peak efficiency is less than $\approx 80\,kV/cm$.

The motion of the electrons in the radiation field is in the form of synchrotron oscillations in the potential well formed by the slow-wave corresponding to the $n = 1$ spatial harmonic. The maximum efficiency is obtained when an electron loses all its initial kinetic energy in the potential well and, in the moving frame, its initial velocity is reversed. The reversal in velocity is attained after a time $\sim \pi/\Omega_{syn0}$, where Ω_{syn0} is the synchrotron frequency. From Eq. (20),

$$\Omega_{syn0} = \left\{ \frac{2\pi}{d} \frac{|e|}{m\gamma_z^3} [A_1 I_0(\kappa_1 r_b) + B_1 K_0(\kappa_1 r_b)] \right\}^{1/2} . \tag{27}$$

In Eq. (27), r_b is the radial coordinate of the beam centroid. In this example the beam is taken to be infinitely-thin and r_b is the r coordinate of the beam, i.e., the distance of the beam from the symmetry axis.

Figure 5 (b) shows the efficiency for a warm, finite-thickness electron beam ($\Delta r_b = 25\,\mu m$). (See Table 1 for other parameters in this example.) The peak efficiency indicated in Fig. 5 (b), $\eta = 0.41\%$, is observed to be smaller than the peak efficiency for the infinitely-thin beam example in Fig. 5 (a).

For a thick beam the synchrotron frequency varies according to the r coordinate of the electrons. As a consequence of their gyromotion, however, the electrons rotate

and sample the transverse profile of the electric field as they cross the interaction region. Therefore, there is a variation in the synchrotron period of the electrons at different distances from the surface of the central conductor. Following the analysis of Ref. 15, it can be shown that the efficiency of a finite-thickness beam is smaller than that of an infinitely-thin beam by the factor $< I_0^{1/2}(\kappa_1 \xi X_b) >$, where I_0 is the modified Bessel function of the first kind of order 0 and $<>$ indicates an average over the random variable ξ. In deriving this result it has been assumed that the electrons gyrate many times as they transit the interaction region; i.e., $\Omega/\Omega_{sym0} \gg 1$, where Ω is the gyration frequency defined following Eq. (12) and Ω_{sym0} is the synchrotron frequency defined in Eq. (27). Inserting the appropriate numerical values we find $< I_0^{1/2}(\kappa_1 \xi X_b) >= 1.3$, which is to be compared with the ratio of the peak efficiencies in Figs. 5 (a) and 5 (b), i.e., $0.59/0.41 = 1.4$.

B. 68 μm Radiation

Beam emittance and energy spread have a deleterious effect on the operation of any free-electron source of radiation. The drop in the peak efficiency observed between Figs. 5 (a) and (b) testifies to this in the case of $\lambda = 45\mu m$. In that example the infinitely-thin beam efficiency is 0.59 %, which is to be compared with the relative axial energy spread on the beam, $\delta\gamma_z/(\gamma - 1) = 0.19\%$, as indicated in Fig. 4 (b). Figures 6 (a) and (b) show the efficiency for the case $\lambda = 68\mu m$. In this example the infinitely-thin beam efficiency is 0.49 %, while $\delta\gamma_z/(\gamma - 1) = 0.46\%$. Figure 6 (b) indicates that in this example, where $\delta\gamma_z/(\gamma - 1)$ is nearly equal to the ideal

beam efficiency, growth of electromagnetic energy from noise is impossible. That is, the oscillator is in the regime of hard excitation.

C. Tuning Characteristics

Figures 7 (a)-(c) summarize the results for a finite-emittance electron beam over the wavelength band 35-55 μm. The limited wavelength band is chosen in order to avoid the hard excitation regime beyond ~ 55 μm. At the short-wavelength end, the large start-oscillation currents along with the relatively high conversion efficiencies [Fig. 7 (a)] lead to the extremely high output power shown in Fig. 7 (b). Figure 7 (c) shows the amplitude, A_0, of the fundamental spatial harmonic at the peak efficiency. As noted in subsection **A**, the actual field in the waveguide gap is much smaller and well below typical breakdown limits.

IV. Conclusions

We have presented design parameters for a hollow beam-coaxial waveguide grating FEL utilizing 105 kV electrons to generate 45 μm radiation and described the characteristics for tuning the source in the wavelength band 35-55 μm. A novel aspect of the configuration is the use of an annular electron beam streaming through a coaxial waveguide. This is expected to avoid the edge effects observed with previous, planar sheet beam, grating experiments. All the design parameters but the efficiency have been obtained from a small-signal analysis of the pendulum equation, which describes the synchrotron oscillations of electrons in the slow-wave structure associated with the corrugated central conductor of the waveguide.

The nonlinear evolution of the electron beam has been analyzed with the aid of a particle simulation code. This code follows the motion of electrons through given fields and permits the determination of the conversion efficiency. The code incorporates the synchrotron and betatron motions of a finite-emittance beam, with allowance for electron gyro-motion in an axial guide magnetic field. Additionally, the effects of self-electric and -magnetic fields are included, although for the design parameters here self-field effects are relatively small.

We have studied and compared the efficiency for two cases, an infinitely-thin beam and a finite-emittance beam. It is shown by means of a numerical example that for sufficiently large emittance the oscillator transitions to the hard excitation regime. When the beam emittance is relatively small, that is, in the soft excitation regime, close agreement between analytical and numerical estimates for the

efficiency is obtained.

The point design and the corresponding tuning characteristics indicate that a far-IR source with output in the kilowatt range is realizable. This source may be made to be extremely compact. The size and capital cost of the accelerator are small and relatively little shielding is required. Similarly, the dimensions of the coaxial waveguide and the magnets for guiding the beam are small. The beam quality requirements are readily achieved in the laboratory. Finally, the electric field at which the optimum efficiency is obtained is well below the threshold for breakdown.

Acknowledgment

This work was supported by the Office of Naval Research.

References

[1] S. J. Smith and E. M. Purcell, "Visible light from localized surface charges moving across a grating," Phys. Rev., vol. 92, p. 1069, 1953.

[2] F. S. Rusin and G. D. Bogomolov, "Generation of electromagnetic oscillations in an open resonator," Zh. Eksp. Teor. Fiz. Pis'ma, vol. 4, pp. 236-239, 1966. [JETP Lett., vol. 4, pp. 160-162, 1966.]

[3] E. I. Nefedov, "Coaxial orotron," Izv. Vyssh. Uchebn. Zaved. Radiofiz., vol. 20, pp. 1740-1743, 1977. [Radiophys. Quantum Electron., vol. 20, pp. 1198-1200, 1977].

[4] K. Mizuno and S. Ono, "The ledatron," in *Infrared and Millimeter Waves*, New York: Academic, 1979, vol. 1, pp. 213-233.

[5] J. M. Wachtel, "Free-electron lasers using the Smith-Purcell effect," J. Appl. Phys., vol. 50, pp. 49-56, 1979.

[6] D. E. Wortman, R. P. Leavitt, H. Dropkin and C. A. Morrison, "Generation of millimeter-wave radiation by means of a Smith-Purcell free-electron laser," Phys. Rev. A, vol. 24, pp. 1150-1153, 1981.

[7] R. P. Leavitt, D. E. Wortman and H. Dropkin, "Millimeter wave orotron oscillation–Part 1: Theory," IEEE J. Quantum Electron., vol. QE-17, pp. 1333-1340, 1981; D. E. Wortman, H. Dropkin and R. P. Leavitt, IEEE J. Quantum Electron., vol. QE-17, pp. 1341-1348, 1981.

[8] D. E. Wortman and R. P. Leavitt, "The orotron," in *Infrared and Millimeter Waves*, New York: Academic, 1983, vol. 7, p. 321-375.

[9] S. D. Korovin, G. A. Mesyats and S. D. Polevin, "Smith-Purcell source of intense millimeter-range radiation," Pis'ma Zh. Tekh. Fiz., vol. 10, pp. 1269-1273, 1984. [Sov. Tech. Phys. Lett., vol. 10, pp. 536-539, 1984.]

[10] E. M. Marshall, P. M. Phillips and J. E. Walsh, "Planar orotron experiments in the millimeter wavelength band," IEEE Trans. Plasma Sci., vol. 16, pp. 199-205, 1988.

[11] E. Garate, R. Cherry, A. Fisher and P. Phillips, "High gain metal grating free-electron laser," J. Appl. Phys., vol. 64, pp. 6618-6625, 1988.

[12] J. E. Walsh, T. L. Buller, B. Johnson, G. Dattoli and F. Ciocci, "Metal-grating far-infrared free-electron lasers," IEEE J. Quantum Elec., vol. QE-21, pp. 920-922, 1985.

[13] G. Doucas, J. H. Mulvey, M. Omori, J. Walsh and M. F. Kimmitt, 'First observation of Smith-Purcell radiation from relativistic electrons," Phys. Rev. Lett., vol. 69, pp. 1761-1764, 1992.

[14] M. J. Moran, "X-ray generation by the Smith-Purcell effect," Phys. Rev. Lett., vol. 69, pp. 2523-2526, 1992.

[15] B. Hafizi, P. Sprangle and P. Serafim, "Nonlinear analysis of a grating free-electron laser," Phys. Rev. A, vol. 45, pp. 8846-8853, 1992.

[16] J. W. Gewartowski and H. A. Watson, *Principles of Electron Tubes*, Princeton: van Nostrand, 1965, sec. 8.7

[17] J. D. Lawson, *The Physics of Charged-Particle Beams*, Oxford: Oxford University Press, 1988, chap. 4.

[18] W. B. Colson, "One-body electron dynamics in a free electron laser," Phys. Lett. A, vol. 64, pp. 190-192, 1977.

[19] A. Yariv, *Quantum Electronics*, New York: Wiley, 1989, sec. 7.4.

Table 1

Wavelength λ	45	μm
Voltage V	105	kV
Current I_b	10.45	A
Radiated Power	4.5	kW
Efficiency η	0.41	%
Guide Magnetic Field B_0	6	T
Beam Emittance	0.8	$\pi - mm - mrad$
Electron Beam Width Δr_b	25	μm
Gain/Pass G	94	%
Resonator Length L_z	1	cm
Grating Pitch d	25	μm
Groove Width s	12.5	μm
Groove Depth b	12.5	μm
Radius of Outer Conductor R	5	mm
Radius of Central Conductor r_g	3	mm
Effective Reflectivity R_{eff}	90	%
Quality Factor Q_L	2661	
Homogeneous Broadening $(\delta\lambda/\lambda)_{hom}$	0.25	%
Inhomogeneous Broadening $(\delta\lambda/\lambda)_{inhom}$	0.07	%

Design parameters for a grating FEL
operating at 45 μm using a 105 kV electron beam

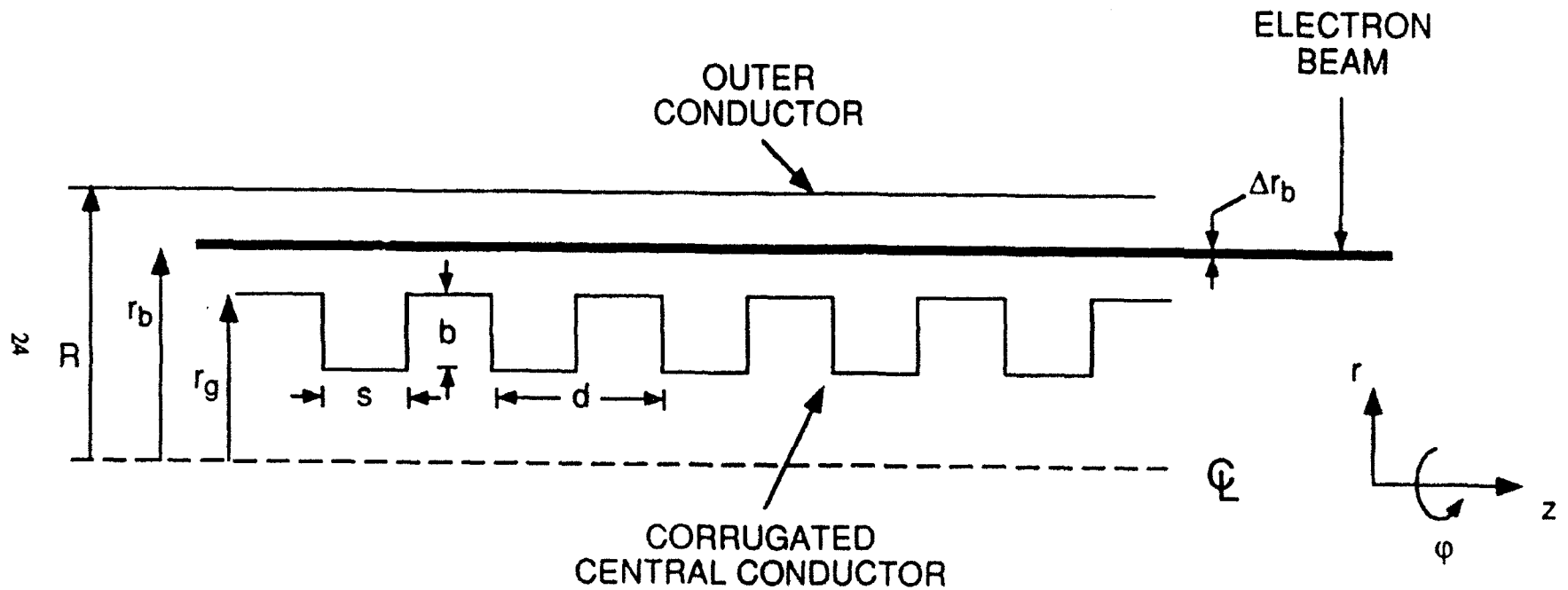

Figure 1: Coaxial waveguide configuration for grating FEL oscillator using annular electron beam.

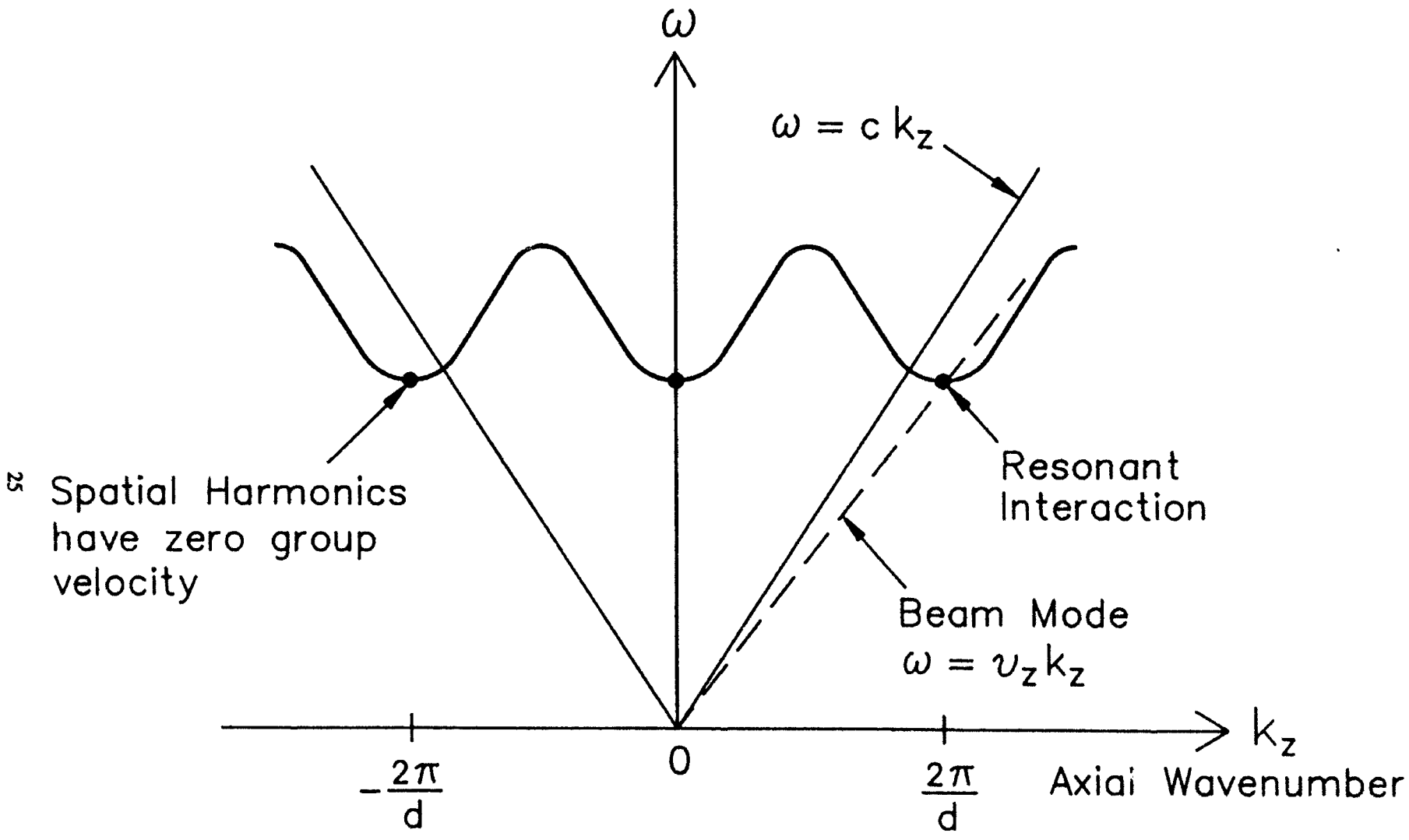

Figure 2: One branch of Brillouin diagram for the three lowest spatial harmonics of oscillator in Fig. 1. Axial wavenumber is denoted by k_z.

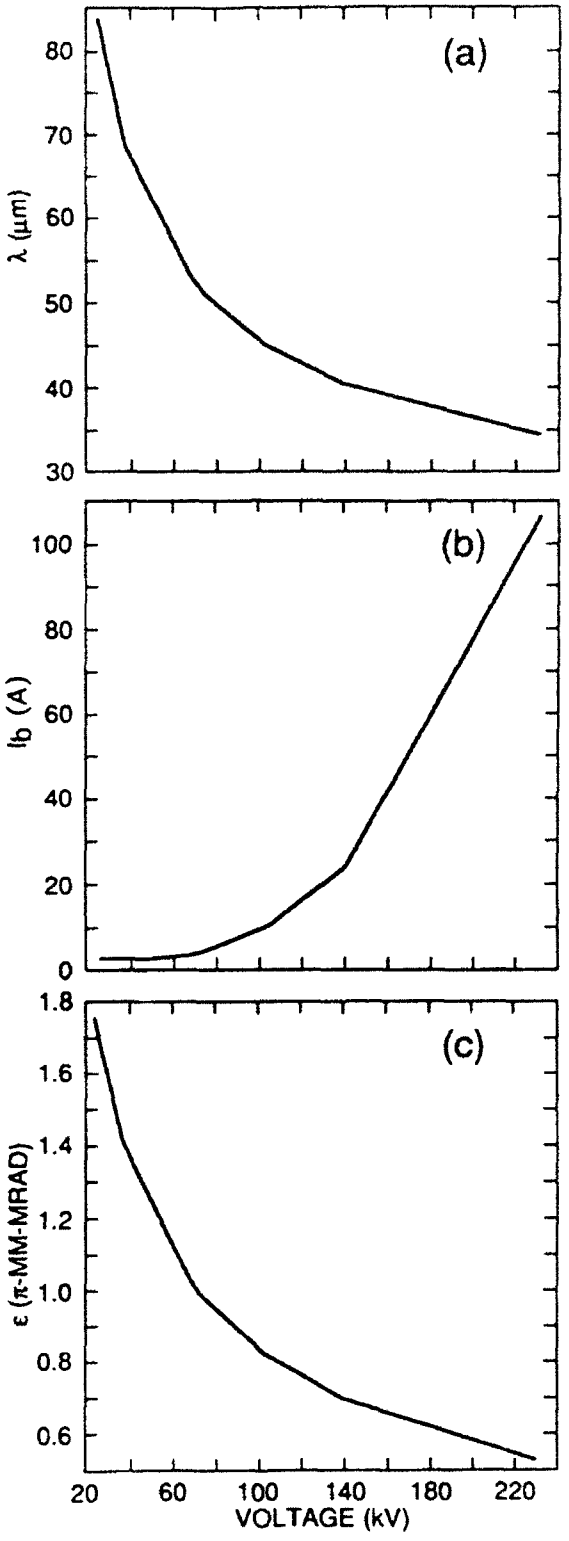

Figure 3: Variation of (a) wavelength, λ, (b) start-oscillation current, I_b, and (c) unnormalized emittance, ϵ with beam voltage.

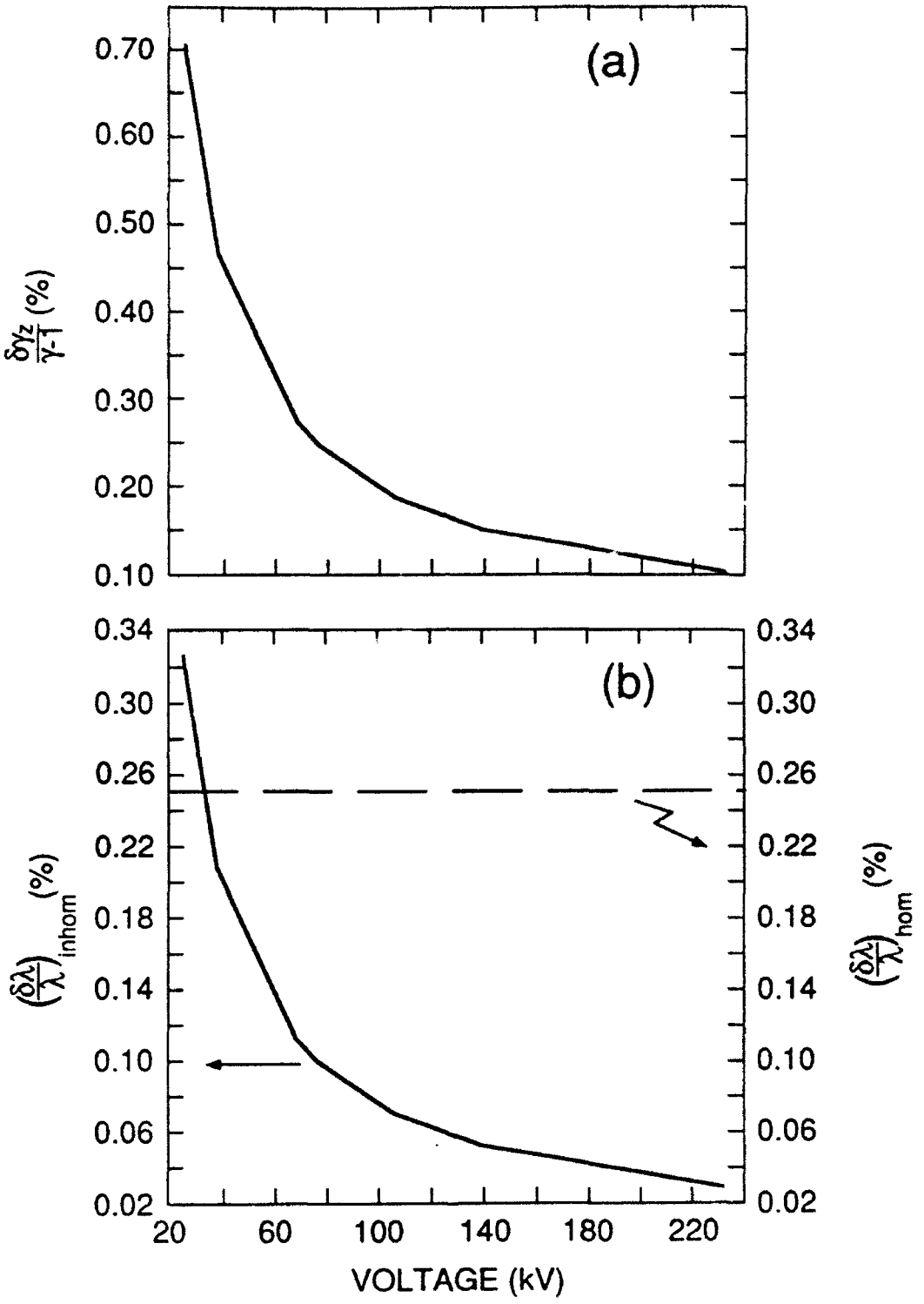

Figure 4: Variation of (a) relative energy spread, $\delta\gamma_z/(\gamma-1)$, (b) homogeneous broadening, $(\delta\lambda/\lambda)_{hom}$, (dashed line) and inhomogeneous broadening, $(\delta\lambda/\lambda)_{inhom}$, (solid line) with beam voltage.

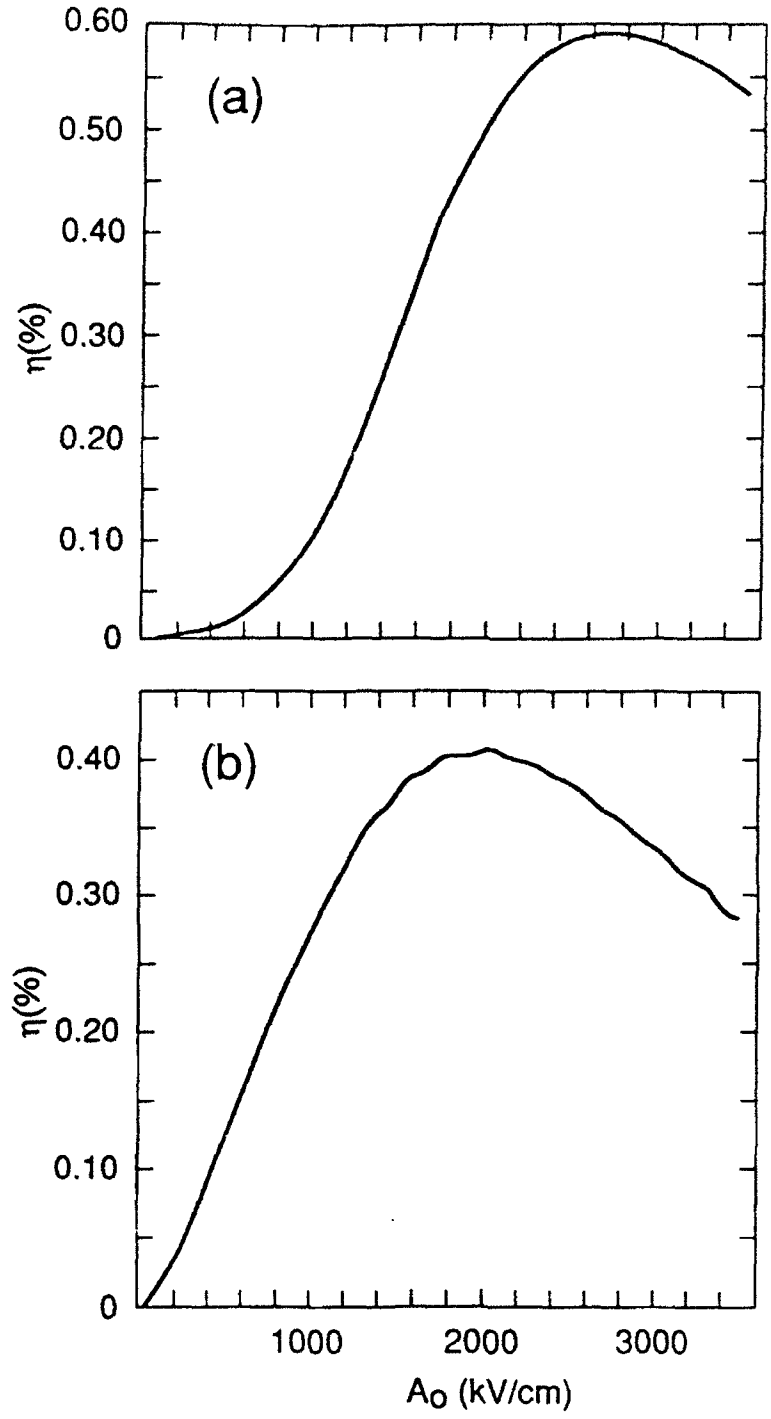

Figure 5: Efficiency, η, versus amplitude of fundamental spatial harmonic, A_0, for $\lambda = 45\,\mu m$ radiation using a 105 kV beam. Beam axis is 12.5 μm above grating surface. (a) Infinitely-thin beam. (b) Finite-thickness beam with full transverse motion ($\Delta r_b = 25\,\mu m$). Maximum electric field in waveguide at peak efficiency is less than $\approx 80\,kV/cm$.

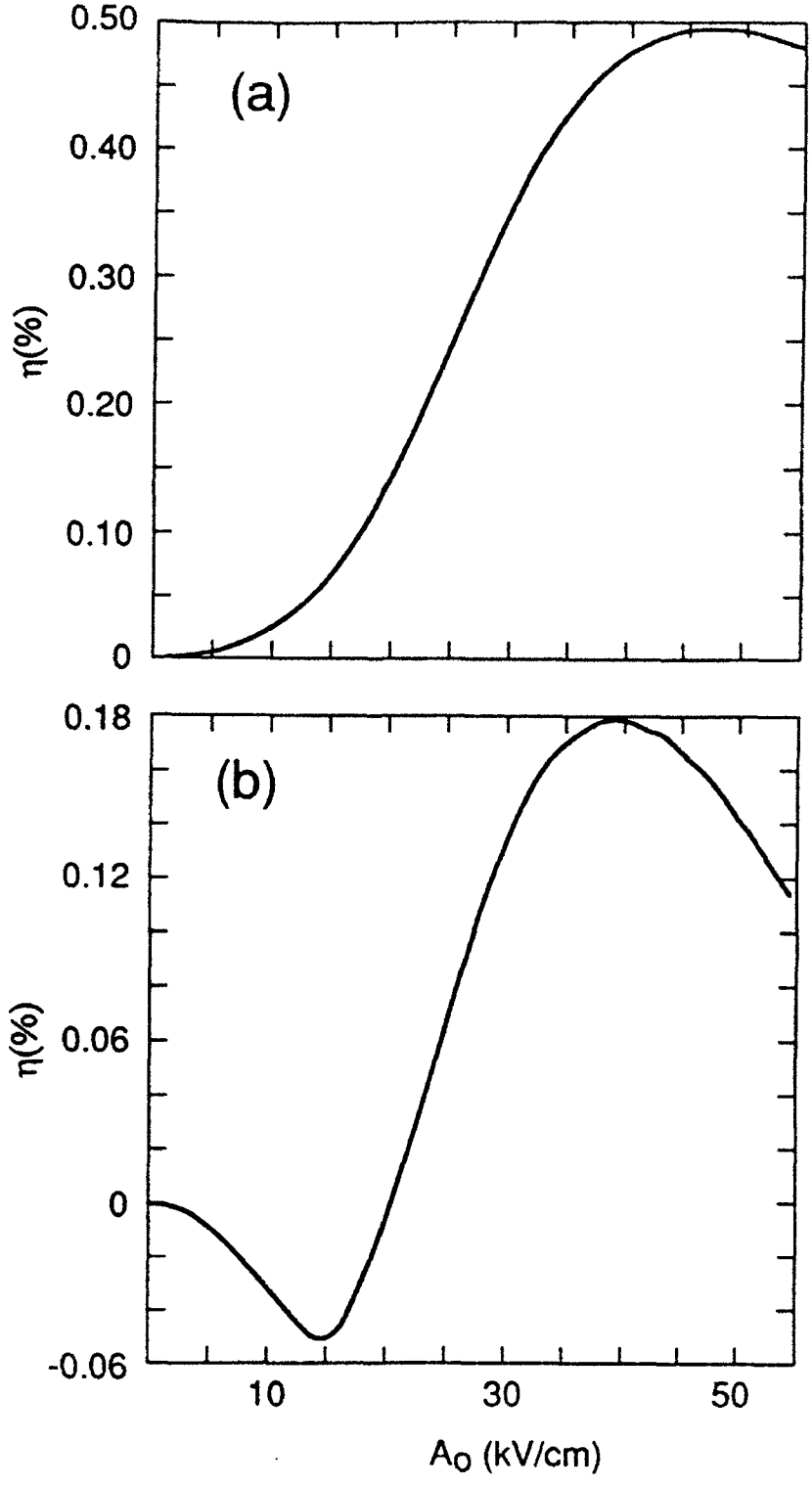

Figure 6: Efficiency, η, versus amplitude of fundamental spatial harmonic, A_0, for $\lambda = 68\,\mu m$ radiation using a 38 kV beam. Beam axis is 12.5 μm above grating surface. (a) Infinitely-thin beam. (b) Finite-thickness beam with full transverse motion ($\Delta r_b = 25\,\mu m$).

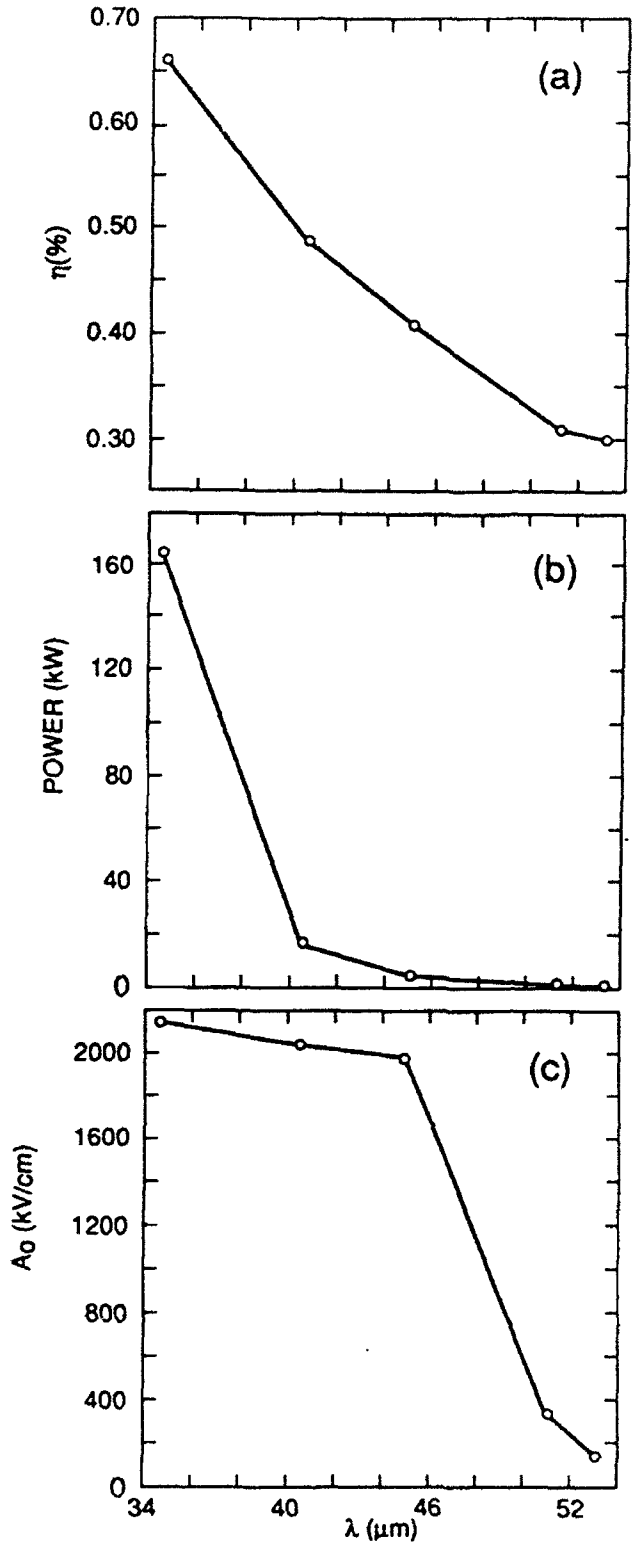

Figure 7: Variation of (a) finite-emittance efficiency, η, (b) output power, and (c) amplitude of fundamental spatial harmonic, A_0, with wavelength, λ. Displayed wavelength band lies in soft excitation regime.